




Article

A Novel SINS/SRS/CNS Multi-Information Fusion Global Autonomous Navigation Method

Bin Zhao ^{1,2}, Qinghua Zeng ^{1,*}, Jianye Liu ¹, Chunlei Gao ², Xiaoling Zhu ¹ and Wei Qiao ¹¹ Navigation Research Center, Nanjing University of Aeronautics & Astronautics, Nanjing 211106, China² School of Air Transportation and Engineering, Nanhang Jincheng College, Nanjing 211156, China

* Correspondence: zengqh@nuaa.edu.cn

Abstract: In order to improve the continuity and smoothness of transpolar flight and optimize autonomous navigation performance, a SINS/SRS/CNS (strapdown inertial navigation system/spectral redshift navigation system/celestial navigation system) multi-information fusion global autonomous navigation method based on parameter conversion was studied for this article. The global autonomous navigation scheme based on multi-information fusion was designed. The principle of spectral redshift navigation was studied. On this basis, the system equations of the SINS/SRS/CNS multi-information fusion global autonomous navigation system were established in the middle–low latitudes and high latitudes. Furthermore, the navigation and filter parameter conversion relationships between the geographic navigation coordinate frame and the grid navigation coordinate frame were derived. The simulation and experiment verified that the SINS/SRS/CNS multi-information fusion global autonomous navigation method with parameter conversion can effectively improve the accuracy and smoothness and realize non-oscillation switching in transpolar navigation. In the vehicle experiment, the proposed algorithm improved the horizontal position accuracy by more than 29% compared with the multi-information fusion global autonomous navigation method without filter parameter conversion.

Keywords: global autonomous navigation; transpolar flight; filter parameter conversion; spectral redshift navigation system



Citation: Zhao, B.; Zeng, Q.; Liu, J.; Gao, C.; Zhu, X.; Qiao, W. A Novel SINS/SRS/CNS Multi-Information Fusion Global Autonomous Navigation Method. *Appl. Sci.* **2022**, *12*, 10862. <https://doi.org/10.3390/app122110862>

Academic Editor: Rosario Pecora

Received: 4 October 2022

Accepted: 24 October 2022

Published: 26 October 2022

Publisher's Note: MDPI stays neutral with regard to jurisdictional claims in published maps and institutional affiliations.



Copyright: © 2022 by the authors. Licensee MDPI, Basel, Switzerland. This article is an open access article distributed under the terms and conditions of the Creative Commons Attribution (CC BY) license (<https://creativecommons.org/licenses/by/4.0/>).

1. Introduction

High-altitude and long-endurance flight requires UAVs (unmanned aerial vehicles) to have global autonomous navigation capability [1]. The unique geographical environment of the polar regions puts forward higher requirements for the continuity and smoothness of navigation. SINS (the strapdown inertial navigation system) is applicable to global navigation because of its concealment, real-time operation, and independence from complex environments. However, with the increase in latitude, the east–north–up navigation coordinate frame extensively used in the middle–low latitudes is ineffective because of meridian convergence [2–4]. Consequently, the transverse geographic coordinate frame that rotates the traditional longitude and latitude lines by 90° and the grid coordinate frame that is based on the Greenwich meridian plane are presently used [5–7]. In addition, the SINS errors gradually accumulate, making it difficult to accomplish a UAV high-precision and long-endurance global flight mission. Consequently, it is essential to introduce other navigation information for SINS correction [8].

In recent years, many studies have been carried out on polar navigation. A fault-tolerant grid SINS/DVL (Doppler velocity log)/USBL (ultra-short baseline) integrated algorithm was proposed to improve the reliability and accuracy of polar navigation for ocean space applications [9]. The integrated navigation scheme of transverse SINS/DVL based on the virtual sphere model was proposed, and the navigation accuracy could meet the requirements of an autonomous underwater vehicle [10]. The rotation modulation

inertial navigation system algorithm under a grid coordinate frame was studied, and the applied basis of polar navigation was established [11]. An interacting dual-model-based adaptive filter was proposed in INS/GNSS/DVL integrated navigation to overcome nonstationary noise and certain non-Gaussian factors, and ship sailing simulations demonstrated that the proposed architecture and algorithms enhanced navigational performance in the Arctic [12]. A SINS/CNS/GPS integrated navigation system that combines the azimuth navigation algorithm and the grid navigation algorithm was obtained, and the feasibility in the high latitudes was verified [13]. Related studies have achieved remarkable results. However, autonomous navigation technology of multi-information fusion for an airborne application background and transregional switching between middle and high latitudes need further research.

To meet the demand for fully autonomous, high-accuracy, and long-endurance navigation, correcting SINS errors with CNS (the celestial navigation system) has already become one research focus of aerospace engineering [14]. The U.S. Air Force has developed various typical airborne SINS/CNS integrated navigation products to meet the requirements of strategic reconnaissance missions [15]. SRS (the spectral redshift navigation system) is a novel autonomous navigation technology that uses the Doppler shift effect of astronomical spectra to realize aircraft navigation with preferable real-time operation and autonomy [16]. The fusion of SINS with SRS and CNS could guarantee the reliability of the navigation system while maintaining a high level of autonomy.

In this article, a SINS/SRS/CNS multi-information fusion global autonomous navigation method based on parameter conversion is proposed. Our main contribution is to establish the SINS/SRS/CNS multi-information fusion system equations in different navigation coordinate frames and to derive the navigation and filter parameter conversion relationships between different coordinate frames, ensuring the high autonomy and precision of the UAV global navigation system. The sections of this article are arranged as follows: The design of the scheme of multi-information fusion global autonomous navigation is detailed in Section 2. Section 3 analyzes the principle of spectral redshift navigation. The system equations of the middle–low-latitude geographic coordinate frame and the high-latitude grid coordinate frame are also established in Section 3. Based on Section 3, Section 4 is devoted to deriving the navigation and filter parameter conversion relationships between different navigation coordinate frames. Section 5 describes the simulation and experiment that were performed to verify the proposed algorithm. Section 6 discusses the main conclusion of this article.

2. Design of the Multi-Information Fusion Global Autonomous Navigation Scheme

For the SINS/SRS/CNS multi-information fusion global autonomous navigation, SINS was selected as the major system, while SRS and CNS were selected as auxiliary systems. The velocity provided by SRS and the latitude and longitude provided by CNS are used to correct the navigation errors of SINS. Moreover, a BA (barometric altimeter) is used to compensate for the inability of CNS to measure altitude.

A high-altitude and long-endurance UAV needs to traverse between polar and nonpolar regions during global flights. Consequently, it is necessary to consider the navigation and filter parameter conversion relationships between different navigation coordinate frames.

In summary, the multi-information fusion global autonomous navigation scheme for UAVs is shown in Figure 1.

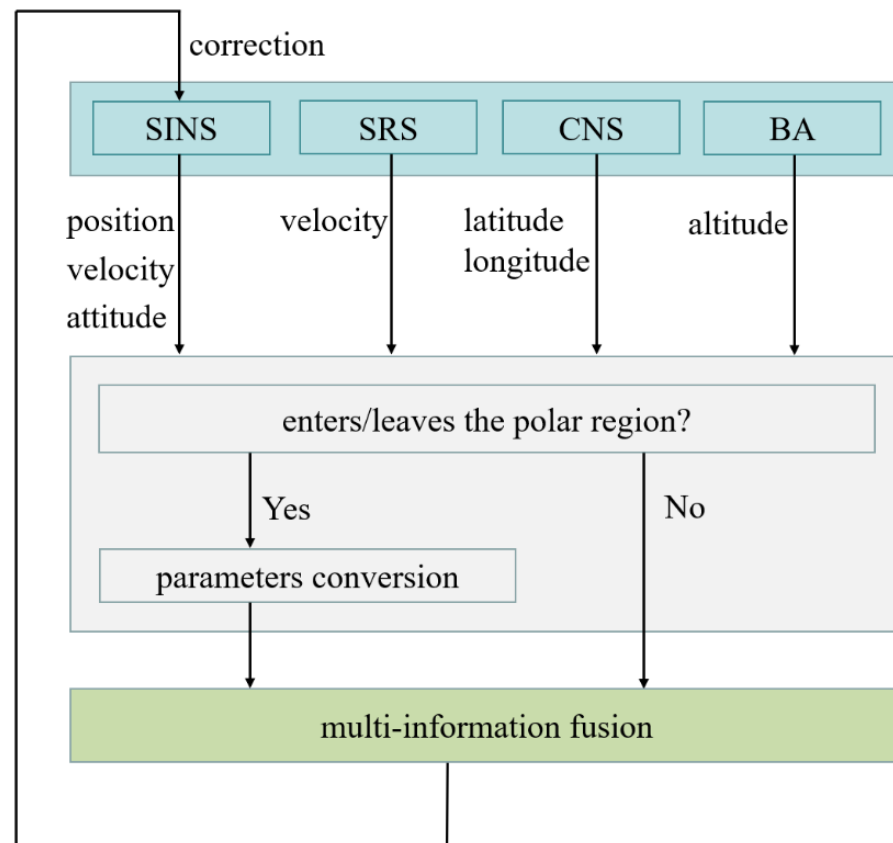


Figure 1. The multi-information fusion global autonomous navigation scheme diagram for UAVs.

3. The Multi-Information Fusion Autonomous Navigation System Based on SINS/SRS/CNS

First, the frames used in this section are defined:

i frame—inertial coordinate frame. It is fixed with the inertial space and can be used as a reference to describe the Earth and carrier angular motion.

g frame—east–north–up geographic coordinate frame. It is the navigation coordinate frame in the nonpolar regions.

e frame—Earth coordinate frame. It is fixed with the Earth and can be used as a reference to describe the carrier position.

b frame—body coordinate frame. The direction relationship between the *b* frame and the navigation system is the carrier attitude.

G frame—grid coordinate frame. It is the navigation coordinate frame in the polar regions. The angle between the grid north and the geographic north is the grid angle, σ .

c frame—calculation coordinate frame. It is the navigation coordinate frame described by SINS, which contains the platform error angle.

The relation diagram for the above frames is shown in Figure 2.

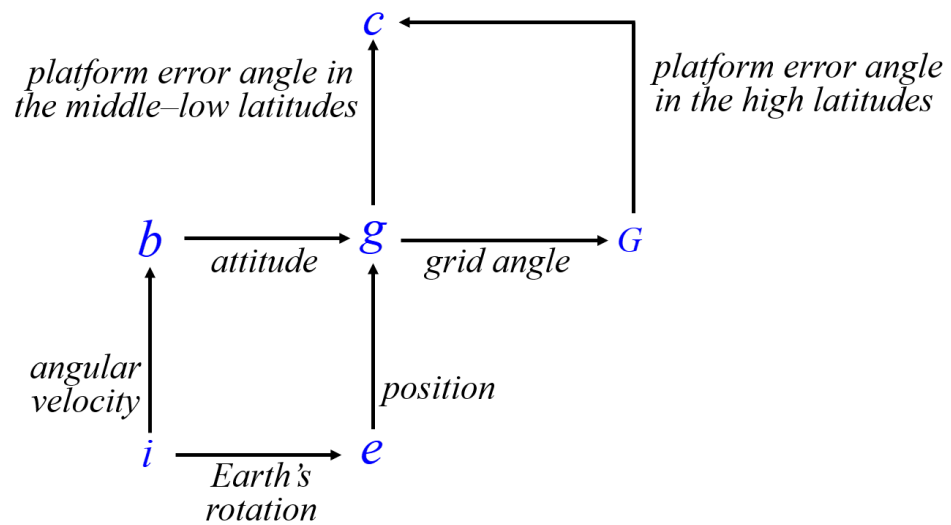


Figure 2. The relation between the frames.

3.1. The Principle of Spectral Redshift Navigation

When the photon frequency emitted by a celestial body produces a color change in the spectrum, the spectrum emitted by the celestial body differs from the spectrum the carrier receives. The redshift is an essential parameter of the spectrum, including the relative velocity. The redshift, z , is defined as:

$$z = \frac{\lambda - \lambda_0}{\lambda_0} = \frac{f_0 - f_m}{f_m} \tag{1}$$

where λ_0 is the initial wavelength of the spectrum lines, λ is the measured wavelength; f_0 is the initial frequency of the spectral lines; and f is the measured frequency.

The redshift equation can be obtained from the equation:

$$1 + z = \frac{f_0}{f_m} = \frac{1 + |v| \cos \theta / c}{\sqrt{1 - |v|^2 / c^2}} \tag{2}$$

where v is the velocity of the carrier relative to the celestial body in the i frame; θ is the angle between the astro-carrier vector and v ; and c is the light velocity.

According to the ephemeris of the celestial bodies and the carrier attitude, combined with the measurement of spectral redshift, the flight velocity of the carrier can be obtained [17,18]. The basic principle of spectral redshift autonomous navigation is as follows. The schematic diagram of spectral redshift navigation is shown in Figure 3:

During flight, the carrier can detect the light signal emitted by the celestial body. From the Doppler principle, it can be known that the spectral frequency received by the carrier is not equal to the frequency the celestial body emitted, so the relative velocity between the carrier and the celestial body can be calculated by measuring the spectral redshift. When the number of non-collinear celestial bodies detected by the carrier is not less than three, the carrier velocity can be obtained by geometrical relations. The solution process is as follows [16,19,20].

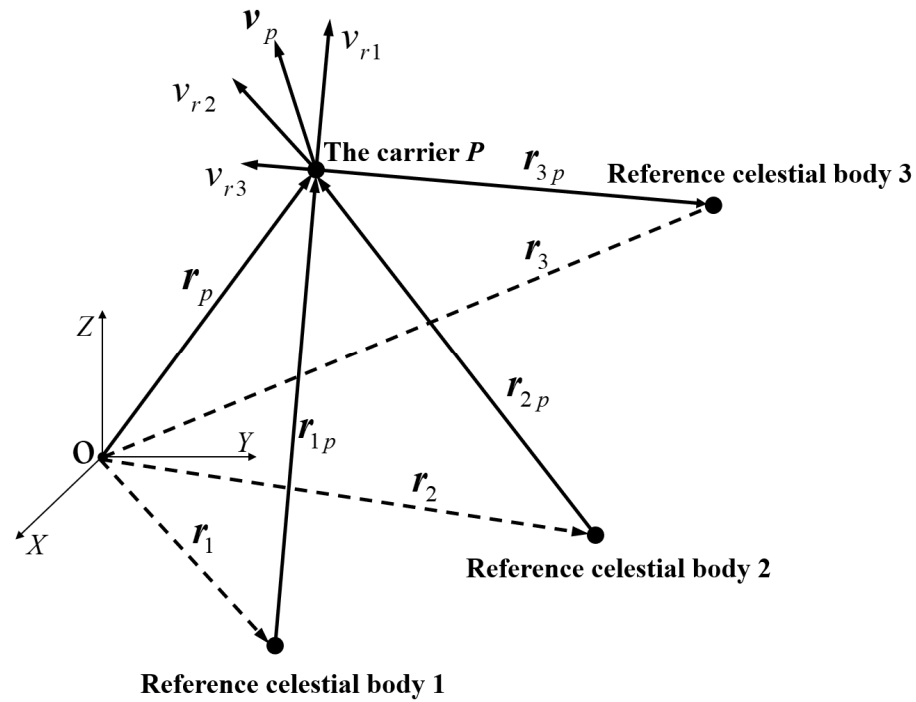


Figure 3. The schematic diagram of spectral redshift navigation, where r_1, r_2, r_3, r_p represent the position vectors of celestial body 1, celestial body 2, celestial body 3, and carrier P in the inertial coordinate system, respectively; r_{1p}, r_{2p}, r_{3p} represent the position vectors from three celestial bodies to the carrier; v_{r1}, v_{r2}, v_{r3} are the radial velocities of the carrier relative to three reference celestial bodies; and v_p is the velocity vector of the carrier in the i frame.

According to Equation (2), when the carrier moves relative to the celestial body, it can be obtained that:

$$|v| \cos \theta = (1 + z) \sqrt{c^2 - |v|^2} - c \tag{3}$$

The above equation is also the radial velocity of the carrier relative to the celestial body:

$$v_r = |v| \cos \theta = (1 + z) \sqrt{c^2 - |v|^2} - c \tag{4}$$

Equation (4) is applied to the first reference celestial body:

$$v_{r1} = (1 + z_1) \sqrt{c^2 - |v_p - v_1|^2} - c \tag{5}$$

where v_{r1} is the radial velocity of the carrier relative to the first reference celestial body; z_1 is the redshift of the carrier relative to the first reference celestial body; v_p is the velocity of the carrier in the i frame; and v_1 is the velocity of the first reference celestial body in the i frame.

The equation group can be listed by selecting three reference celestial bodies:

$$\begin{cases} v_{r1} = (1 + z_1) \sqrt{c^2 - |v_p - v_1|^2} - c \\ v_{r2} = (1 + z_2) \sqrt{c^2 - |v_p - v_2|^2} - c \\ v_{r3} = (1 + z_3) \sqrt{c^2 - |v_p - v_3|^2} - c \end{cases} \tag{6}$$

According to the geometrical relation, v_p and v_{r1}, v_{r2}, v_{r3} satisfy:

$$\begin{cases} v_{r1} = (v_p - v_1) \cdot u_1 \\ v_{r2} = (v_p - v_2) \cdot u_2 \\ v_{r3} = (v_p - v_3) \cdot u_3 \end{cases} \tag{7}$$

where v_1, v_2, v_3 are the velocities of reference celestial bodies in the i frame, obtained from the ephemeris, and u_1, u_2, u_3 are the unit vectors between the celestial bodies and the carrier, observed by the star sensor.

By substituting Equation (7) into Equation(6), we obtain:

$$\begin{cases} (v_p - v_1) \cdot u_1 - (1 + z_1)\sqrt{c^2 - |v_p - v_1|^2} + c = 0 \\ (v_p - v_2) \cdot u_2 - (1 + z_2)\sqrt{c^2 - |v_p - v_2|^2} + c = 0 \\ (v_p - v_3) \cdot u_3 - (1 + z_3)\sqrt{c^2 - |v_p - v_3|^2} + c = 0 \end{cases} \tag{8}$$

Then, the carrier velocity in the i frame can be obtained.

The core equipment of SRS is the optical spectrum instrumentation. The spectral parameters can be measured by the optical spectrum instrumentation. Then, the redshift and the carrier velocity can be calculated. The calculated principle shows that the carrier velocity is obtained by geometrical relations, not by circulative iteration. This means that its error would not accumulate over time, and the correlation time is short. Therefore, the error of SRS can be regarded as white noise, and related studies have been conducted in this way [16,19,20].

3.2. The System Equations of the SINS/SRS/CNS Multi-Information Fusion Autonomous Navigation System in the Middle-Low Latitudes

3.2.1. State Equations

In the middle-low latitudes, the g frame was chosen as the navigation coordinate frame. The SINS error equations in the g frame can be obtained as follows [21].

The mathematical platform error angle equation can be denoted as:

$$\dot{\Phi}^g = \Phi^g \times (\omega_{ie}^g + \omega_{eg}^g) + (\delta\omega_{ie}^g + \delta\omega_{eg}^g) - C_b^g \epsilon^b \tag{9}$$

where Φ^g is the mathematical platform error angle in the g frame; ω_{ie}^g is the projection of the Earth's rotation angular velocity, ω_{ie} , in the g frame; ω_{eg}^g is the angular velocity of the g frame to the e frame, projected in the g frame; $\delta\omega_{ie}^g$ and $\delta\omega_{eg}^g$ are the errors of ω_{ie}^g and ω_{eg}^g ; C_b^g is the direction cosine matrix from the b frame to the g frame; and ϵ^b is the gyroscope drift in the b frame.

The velocity error equation can be denoted as:

$$\delta\dot{v}^g = f^g \times \Phi^g - (2\delta\omega_{ie}^g + \delta\omega_{eg}^g) \times v^g - (2\omega_{ie}^g + \omega_{eg}^g) \times \delta v^g + C_b^g \nabla^b \tag{10}$$

where δv^g is the velocity error in the g frame; f^g represents the specific force in the g frame; and ∇^b is the accelerators drift in the b frame.

The position error, δp^g , comprises the latitude error, δL ; the longitude error, $\delta \lambda$; and the altitude error, δh . The equations of position error are as follows:

$$\begin{cases} \delta\dot{L} = \frac{\delta v_N}{R_M + h} \\ \delta\dot{\lambda} = \frac{\delta v_E}{R_N + h} \sec L + \frac{v_E}{R_N + h} \sec L \tan L \delta L \\ \delta\dot{h} = \delta v_U \end{cases} \tag{11}$$

where R_M and R_N are the radii of curvatures in meridian and prime vertical, respectively, and V_E and V_N are the east velocity and north velocity, respectively.

The gyroscope and accelerator drift error equations can be denoted as

$$\begin{cases} \dot{\boldsymbol{\varepsilon}}^b = 0 \\ \dot{\nabla}^b = 0 \end{cases} \tag{12}$$

According to Equations (9)–(12), select $\boldsymbol{\Phi}^g, \delta v^g, \delta p^g, \boldsymbol{\varepsilon}^b$, and ∇^b as the state vector:

$$\mathbf{X}^g(t) = [\boldsymbol{\Phi}^g \quad \delta v^g \quad \delta p^g \quad \boldsymbol{\varepsilon}^b \quad \nabla^b]^T \tag{13}$$

Then, the state equation of the SINS/SRS/CNS multi-information fusion autonomous navigation system in the middle–low latitudes can be established:

$$\dot{\mathbf{X}}^g(t) = \mathbf{A}^g(t)\mathbf{X}^g(t) + \mathbf{G}^g(t)\mathbf{W}^g(t) \tag{14}$$

where $\mathbf{X}^g(t)$ is the state vector; $\mathbf{A}^g(t)$ is the state transition matrix; $\mathbf{G}^g(t)$ is the system noise coefficient matrix; and $\mathbf{W}^g(t)$ is the system noise vector.

3.2.2. Measurement Equations

There are two sets of measurements: one is the SINS/SRS velocity measurement, and the other is the SINS/CNS position measurement.

(1) SINS/SRS velocity measurement

Given that the velocity provided by SRS is in the i frame, converting it to the g frame in the middle–low latitudes is essential:

$$\mathbf{v}_{SRS}^g = \mathbf{C}_i^g \mathbf{v}_p = \mathbf{C}_e^g \mathbf{C}_i^e \mathbf{v}_p \tag{15}$$

where \mathbf{C}_i^g is the direction cosine matrix from the i frame to the g frame; \mathbf{C}_i^e is the direction cosine matrix from the i frame to the e frame; \mathbf{C}_e^g is the direction cosine matrix from the e frame to the g frame; and \mathbf{v}_{SRS}^g is the velocity in the g frame calculated by SRS.

The velocity differences between SINS and SRS were chosen as one measurement to construct the velocity measurement equation:

$$\mathbf{Z}_v^g(t) = \mathbf{v}_{SINS}^g - \mathbf{v}_{SRS}^g = \mathbf{H}_v^g(t)\mathbf{X}^g(t) + \mathbf{V}_v^g(t) \tag{16}$$

where \mathbf{v}_{SINS}^g is the velocity in the g frame calculated by SINS; $\mathbf{H}_v^g(t) = [0_{3 \times 3} \quad \text{diag}[1 \ 1 \ 1] \quad 0_{3 \times 9}]$ is the measurement matrix of the velocity; and $\mathbf{V}_v^g(t)$ is the velocity noise.

(2) SINS/CNS position measurement

The position differences between SINS, CNS, and BA were selected as the other measurement to construct the position measurement equation:

$$\mathbf{Z}_p^g(t) = \begin{bmatrix} L_{SINS} - L_{CNS} \\ \lambda_{SINS} - \lambda_{CNS} \\ h_{SINS} - h_{BA} \end{bmatrix} = \mathbf{H}_p^g(t)\mathbf{X}^g(t) + \mathbf{V}_p^g(t) \tag{17}$$

where $L_{SINS}, \lambda_{SINS}, h_{SINS}$ are the latitude, longitude, and altitude obtained by SINS; L_{CNS}, λ_{CNS} are the latitude and longitude obtained by CNS; h_{BA} is the altitude obtained by BA; $\mathbf{H}_p^g(t) = [0_{3 \times 6} \quad \text{diag}[1 \ 1 \ 1] \quad 0_{3 \times 6}]$ is the measurement matrix of the position; and $\mathbf{V}_p^g(t)$ is the position noise.

3.3. The System Equations of the SINS/SRS/CNS Multi-Information Fusion Autonomous Navigation System in the High Latitudes

3.3.1. State Equations

In the high latitudes, the G frame was selected as the navigation coordinate frame. The coordinates in the e frame are used to represent the position of the UAV. Therefore, the error equations are as follows [9]:

$$\begin{cases} \dot{\Phi}^G = \Phi^G \times (\omega_{ie}^G + \omega_{eG}^G) + C_v \delta v^G - C_b^G \varepsilon^b \\ \delta \dot{v}^G = f^G \times \Phi^G + (v^G \times C_v - (2\omega_{ie}^G + \omega_{eG}^G) \times) \delta v^G + C_b^G \nabla^b \\ \delta \dot{P}^e = C_G^e \delta v^G - C_G^e (v^G \times) C_P \delta P^e \end{cases} \quad (18)$$

where Φ^G is the mathematical platform error angle in the G frame; v^G is the velocity in the G frame, and δv^G is the error; δP^e is the position error in the e frame; ω_{ie}^G is the projection of the Earth's rotation angular velocity, ω_{ie} , in the G frame; ω_{eG}^G is the angular velocity of the G frame to the e frame, projected in the G frame; f^G represents the specific force in the G frame; C_b^G is the direction cosine matrix from the b frame to the G frame; C_G^e is the direction cosine matrix from the G frame to the e frame;

$$C_v = \frac{1}{\sqrt{(R_M+h)(R_N+h)}} \begin{bmatrix} 0 & -1 & 0 \\ 1 & 0 & 0 \\ 0 & -\cot L \sin \sigma & 0 \end{bmatrix}; \sigma \text{ is the angle between the grid north and}$$

the geographic north; $C_P = \frac{\xi}{\sqrt{(R_M+h)(R_N+h)}} \begin{bmatrix} \sin L & 0 & -\cos \lambda \cos L \\ \sin \lambda \sin L \cos^2 L & 1/\xi^2 & -\sin \lambda \sin L \cos L \\ \cos L \sin L \sin \lambda & 0 & -\cos^2 L \sin \lambda \cos \lambda \end{bmatrix}$,

and $\xi = \frac{1}{\sqrt{1 - \cos^2 L \sin^2 \lambda}}$.

The gyroscope and accelerometer drift error equations are the same as Equation (12).

According to Equations (18) and (12), select Φ^G , δv^G , δP^e , ε^b , and ∇^b as the state vector:

$$X^G(t) = [\Phi^G \quad \delta v^G \quad \delta p^e \quad \varepsilon^b \quad \nabla^b]^T \quad (19)$$

Then, the state equation of the SINS/SRS/CNS multi-information fusion autonomous navigation system in the high latitudes can be established:

$$\dot{X}^G(t) = A^G(t)X^G(t) + G^G(t)W^G(t) \quad (20)$$

where $X^G(t)$ is the state vector; $A^G(t)$ is the state transition matrix; $G^G(t)$ is the system noise coefficient matrix; and $W^G(t)$ is the system noise vector.

3.3.2. Measurement Equations

(1) SINS/SRS velocity measurement

In the high latitudes, it is required to convert the velocity in the i frame calculated by SRS to the G frame:

$$v_{SRS}^G = C_i^G v_p = C_e^G C_i^e v_p \quad (21)$$

where C_i^G is the direction cosine matrix from the i frame to the G frame; C_e^G is the direction cosine matrix from the e frame to the G frame; and v_{SRS}^G is the velocity in the G frame calculated by SRS.

The velocity differences between SINS and SRS were chosen as one measurement to construct the velocity measurement equation:

$$Z_v^G(t) = v_{SINS}^G - v_{SRS}^G = H_v^G(t)X^G(t) + V_v^G(t) \quad (22)$$

where v_{SINS}^G is the velocity in the G frame calculated by SINS; $H_v^G(t) = [0_{3 \times 3} \quad \text{diag}[1 \quad 1 \quad 1] \quad 0_{3 \times 9}]$ is the measurement matrix of the velocity; and $V_v^G(t)$ is the velocity noise.

(2) SINS/CNS position measurement

In the state equations of the high latitudes, the UAV position is represented by the coordinates in the e frame. Therefore, it is necessary to convert the latitude and longitude from CNS and the altitude from BA to the e frame:

$$\begin{cases} x_{CNS} = (R_N + h_{BA}) \cos L_{CNS} \cos \lambda_{CNS} \\ y_{CNS} = (R_N + h_{BA}) \cos L_{CNS} \sin \lambda_{CNS} \\ z_{CNS} = [R_N(1 - f^2) + h_{BA}] \sin L_{CNS} \end{cases} \quad (23)$$

where x_{CNS} , y_{CNS} , z_{CNS} are the position coordinates in the e frame obtained by CNS and BA.

The position differences between SINS, CNS, and BA in the e frame were selected as the other measurement:

$$\mathbf{Z}_p^G(t) = \begin{bmatrix} x_{SINS} - x_{CNS} \\ y_{SINS} - y_{CNS} \\ z_{SINS} - z_{CNS} \end{bmatrix} = \mathbf{H}_p^G(t) \mathbf{X}^G(t) + \mathbf{V}_p^G(t) \quad (24)$$

where x_{SINS} , y_{SINS} , z_{SINS} are the position coordinates in the e frame obtained by SINS, $\mathbf{H}_p^G(t) = [0_{3 \times 6} \quad \text{diag}[1 \quad 1 \quad 1] \quad 0_{3 \times 6}]$ is the measurement matrix of the position; and $\mathbf{V}_p^G(t)$ is the position noise.

4. Parameter Conversion of the SINS/SRS/CNS Multi-Information Fusion Autonomous Navigation System

4.1. Navigation Parameter Conversion

Different navigation coordinate frames are adopted for polar regions and nonpolar regions. Therefore, the navigation parameters need to be switched between the g frame and the G frame during long-duration and transpolar flights.

\mathbf{C}_g^G is the direction cosine matrix from the g frame to the G frame, and its transpose matrix \mathbf{C}_G^g is the direction cosine matrix from the G frame to the g frame:

$$\mathbf{C}_g^G = \begin{bmatrix} \cos \sigma & -\sin \sigma & 0 \\ \sin \sigma & \cos \sigma & 0 \\ 0 & 0 & 1 \end{bmatrix} \quad (25)$$

When the UAV enters the polar regions, the navigation coordinate frame switches from the g frame to the G frame. The polar attitude matrix, \mathbf{C}_b^G , and the polar velocity, \mathbf{v}^G , can be obtained by \mathbf{C}_g^G :

$$\begin{cases} \mathbf{C}_b^G = \mathbf{C}_g^G \mathbf{C}_b^g \\ \mathbf{v}^G = \mathbf{C}_g^G \mathbf{v}^g \end{cases} \quad (26)$$

On the other hand, when the UAV leaves the polar regions, the navigation coordinate frame switches from the G frame to the g frame. The nonpolar attitude matrix, \mathbf{C}_b^g , and the nonpolar velocity, \mathbf{v}^g , can be obtained by \mathbf{C}_G^g :

$$\begin{cases} \mathbf{C}_b^g = \mathbf{C}_G^g \mathbf{C}_b^G \\ \mathbf{v}^g = \mathbf{C}_G^g \mathbf{v}^G \end{cases} \quad (27)$$

The conversion relationship between the position coordinates in the e frame and latitude, longitude, and altitude can be obtained from Equation (23).

4.2. Filter Parameter Conversion

The navigation coordinate frame switches while the UAV enters/leaves the polar regions, and the filter structure and parameters also change. The system equations in the polar/nonpolar regions were established (Section 3), and the coefficient matrices in different

coordinate frames were also determined. The system noise and measurement noise are only related to the sensor accuracy, not to the navigation coordinate frame. Beyond that, to switch between the different system equations, it is necessary to convert the filter state vector and the covariance matrix.

By comparing Equations (13) and (19), it can be known that the inertial sensor errors, ϵ^b and ∇^b , are the same in the g frame and the G frame, so no conversion is required.

The conversion relationship between Φ^g and Φ^G can be derived as follows.

Due to the calculation error, the navigation coordinate frame described by SINS is the c frame, containing the platform error angle. The platform error angle, Φ^G , relative to the G frame is usually a slight angle, so the first-order approximation is feasible. It can be deduced that:

$$C_G^c = I - (\Phi^G \times) \tag{28}$$

Then,

$$\delta C_b^G = C_b^c - C_b^G = C_G^c C_b^G - C_b^G = -(\Phi^G \times) C_b^G \tag{29}$$

Derive both sides of $C_b^G = C_g^G C_b^g$

$$\delta C_b^G = \delta C_g^G C_b^g + C_g^G \delta C_b^g = -(\Phi_{gG}^G \times) C_g^G C_b^g - C_g^G (\Phi^g \times) C_b^g = -(\Phi_{gG}^G \times) C_b^G - C_g^G (\Phi^g \times) C_g^G C_b^g \tag{30}$$

where $\Phi_{gG}^G = [0 \ 0 \ -\delta\sigma]^T$; $\delta\sigma = \frac{\sin\sigma \cos\sigma \cos L}{\sin L} \delta L + \frac{1-\cos^2\sigma \cos^2 L}{\sin L} \delta\lambda$.

By comparing Equations (29) and (30), we can obtain:

$$(\Phi^G \times) = C_g^G (\Phi^g \times) C_g^G + (\Phi_{gG}^G \times) \tag{31}$$

This can be reorganized as:

$$\begin{aligned} \Phi^G &= C_g^G \Phi^g + \Phi_{gG}^G = C_g^G \Phi^g + \begin{bmatrix} 0 \\ 0 \\ -\delta\sigma \end{bmatrix} = C_g^G \Phi^g - \begin{bmatrix} 0 \\ 0 \\ \frac{\sin\sigma \cos\sigma \cos L}{\sin L} \delta L + \frac{1-\cos^2\sigma \cos^2 L}{\sin L} \delta\lambda \end{bmatrix} \\ &= C_g^G \Phi^g - \begin{bmatrix} 0 & 0 & 0 \\ 0 & 0 & 0 \\ \frac{\sin\sigma \cos\sigma \cos L}{\sin L} & \frac{1-\cos^2\sigma \cos^2 L}{\sin L} & 0 \end{bmatrix} \begin{bmatrix} \delta L \\ \delta\lambda \\ \delta h \end{bmatrix} \\ &= C_g^G \Phi^g - \begin{bmatrix} 0 & 0 & 0 \\ 0 & 0 & 0 \\ \frac{\sin\sigma \cos\sigma \cos L}{\sin L} & \frac{1-\cos^2\sigma \cos^2 L}{\sin L} & 0 \end{bmatrix} \delta p^g \\ &\triangleq C_g^G \Phi^g - T_1 \delta p^g \end{aligned} \tag{32}$$

The conversion relationship between δv^g and δv^G is as follows:

$$\begin{aligned} \delta v^G &= C_g^G \delta v^g + \delta C_g^G v^g = C_g^G \delta v^g - (\Phi_{gG}^G \times) C_g^G v^g = C_g^G \delta v^g - \left[\begin{pmatrix} 0 \\ 0 \\ -\delta\sigma \end{pmatrix} \times \right] C_g^G v^g \\ &= C_g^G \delta v^g - \begin{bmatrix} 0 & \delta\sigma & 0 \\ -\delta\sigma & 0 & 0 \\ 0 & 0 & 0 \end{bmatrix} \begin{bmatrix} \cos\sigma & -\sin\sigma & 0 \\ \sin\sigma & \cos\sigma & 0 \\ 0 & 0 & 1 \end{bmatrix} \begin{bmatrix} v_E \\ v_N \\ v_U \end{bmatrix} = C_g^G \delta v^g + \begin{bmatrix} -\sin\sigma \cdot v_E - \cos\sigma \cdot v_N \\ \cos\sigma \cdot v_E - \sin\sigma \cdot v_N \\ 0 \end{bmatrix} \delta\sigma \\ &= C_g^G \delta v^g + \begin{bmatrix} -\sin\sigma \cdot v_E - \cos\sigma \cdot v_N \\ \cos\sigma \cdot v_E - \sin\sigma \cdot v_N \\ 0 \end{bmatrix} \begin{bmatrix} \frac{\sin\sigma \cos\sigma \cos L}{\sin L} & \frac{1-\cos^2\sigma \cos^2 L}{\sin L} & 0 \end{bmatrix} \begin{bmatrix} \delta L \\ \delta\lambda \\ \delta h \end{bmatrix} \\ &= C_g^G \delta v^g + \begin{bmatrix} -\sin\sigma \cdot v_E - \cos\sigma \cdot v_N \\ \cos\sigma \cdot v_E - \sin\sigma \cdot v_N \\ 0 \end{bmatrix} \begin{bmatrix} \frac{\sin\sigma \cos\sigma \cos L}{\sin L} & \frac{1-\cos^2\sigma \cos^2 L}{\sin L} & 0 \end{bmatrix} \delta p^g \\ &\triangleq C_g^G \delta v^g + T_2 \delta p^g \end{aligned} \tag{33}$$

The position in the middle–low latitudes is expressed by latitude, longitude, and altitude, with the error of $\delta p^s = [\delta L \quad \delta \lambda \quad \delta h]^T$. Meanwhile, the position in the high latitudes is expressed by the coordinates in the e frame, with the error of $\delta p^e = [\delta x \quad \delta y \quad \delta z]^T$.

Depending on the relation between latitude, longitude, altitude and the coordinates in the e frame described in Equation (23), it can be obtained that:

$$\begin{cases} \delta x = \delta[(R_N + h) \cos L \cos \lambda] = (R_N + h)(-\sin L \cos \lambda \delta L - \cos L \sin \lambda \delta \lambda) + \cos L \cos \lambda \delta h \\ \delta y = \delta[(R_N + h) \cos L \sin \lambda] = (R_N + h)(-\sin L \sin \lambda \delta L + \cos L \cos \lambda \delta \lambda) + \cos L \sin \lambda \delta h \\ \delta z = \delta[[R_N(1 - f^2) + h] \sin L] = [R_N(1 - f^2) + h] \cos L \delta L + \sin L \delta h \end{cases} \quad (34)$$

Equation (34) can be written as:

$$\delta p^e = \begin{bmatrix} -(R_N + h) \sin L \cos \lambda & -(R_N + h) \cos L \sin \lambda & \cos L \cos \lambda \\ -(R_N + h) \sin L \sin \lambda & (R_N + h) \cos L \cos \lambda & \cos L \sin \lambda \\ [R_N(1 - f^2) + h] \cos L & 0 & \sin L \end{bmatrix} \delta p = T_3 \delta p^s \quad (35)$$

When the UAV enters the polar regions, the navigation coordinate frame switches from the g frame to the G frame. Combining Equations (32), (33), and (35), the polar state vector can be obtained as:

$$X^G(t) = \begin{bmatrix} C_g^G & 0 & -T_1 & 0 & 0 \\ 0 & C_g^G & T_2 & 0 & 0 \\ 0 & 0 & T_3 & 0 & 0 \\ 0 & 0 & 0 & I_{3 \times 3} & 0 \\ 0 & 0 & 0 & 0 & I_{3 \times 3} \end{bmatrix} X^g(t) = \Phi X^g(t) \quad (36)$$

According to the definition of the variance matrix and Equation (36):

$$\begin{aligned} P^G(t) &= E \left\{ \left(X^G(t) - \hat{X}^G(t) \right) \left(X^G(t) - \hat{X}^G(t) \right)^T \right\} = E \left\{ \left(\Phi X^g(t) - \Phi \hat{X}^g(t) \right) \left(\Phi X^g(t) - \Phi \hat{X}^g(t) \right)^T \right\} \\ &= E \left\{ \Phi \left(X^g(t) - \hat{X}^g(t) \right) \left(X^g(t) - \hat{X}^g(t) \right)^T \Phi^T \right\} = \Phi E \left\{ \left(X^g(t) - \hat{X}^g(t) \right) \left(X^g(t) - \hat{X}^g(t) \right)^T \right\} \Phi^T \\ &= \Phi P^g(t) \Phi^T \end{aligned} \quad (37)$$

where $P^g(t)$ is the covariance matrix in the g frame and $P^G(t)$ is the covariance matrix in the G frame.

Similarly, when the UAV leaves the polar regions, the state vector and covariance matrix in the g frame can be obtained as:

$$\begin{cases} X^g(t) = \Phi^{-1} X^G(t) \\ P^g(t) = \Phi^{-1} P^G(t) (\Phi^T)^{-1} \end{cases} \quad (38)$$

In summary, it is only necessary to switch the navigation coordinate frame in the software and algorithm according to the calculated latitude. The navigation hardware devices do not need any conversion.

5. Experiment and Discussion

5.1. Simulation and Analysis

To validate the performance of the SINS/SRS/CNS multi-information fusion global autonomous navigation method, a simulation and an analysis were performed, combined with the system equations established in Section 3. The parameters of the navigation sensors for the simulation are shown in Table 1.

Table 1. Sensor rate settings.

Parameters	Value
Gyro constant bias (deg/h)	0.01
Accelerometer constant bias (ug)	100
Gyro angular random walk (deg/sqrt(h))	0.001
Accelerometer velocity random walk (ug/sqrt(Hz))	10
CNS position error (m)	20
BA altitude error (m)	10
SRS velocity error (m/s)	0.5

The latitude of the original location was 87.5° . The UAV flew at uniform velocity and arrived at latitude 88° at 212 s. The navigation coordinate frame was switched from the g frame to the G frame. The proposed SINS/SRS/CNS multi-information fusion autonomous navigation method with filter parameter conversion was compared with that without filter parameter conversion. Figure 4a–c demonstrate the position error, velocity error, and attitude error generated by these two methods, respectively.

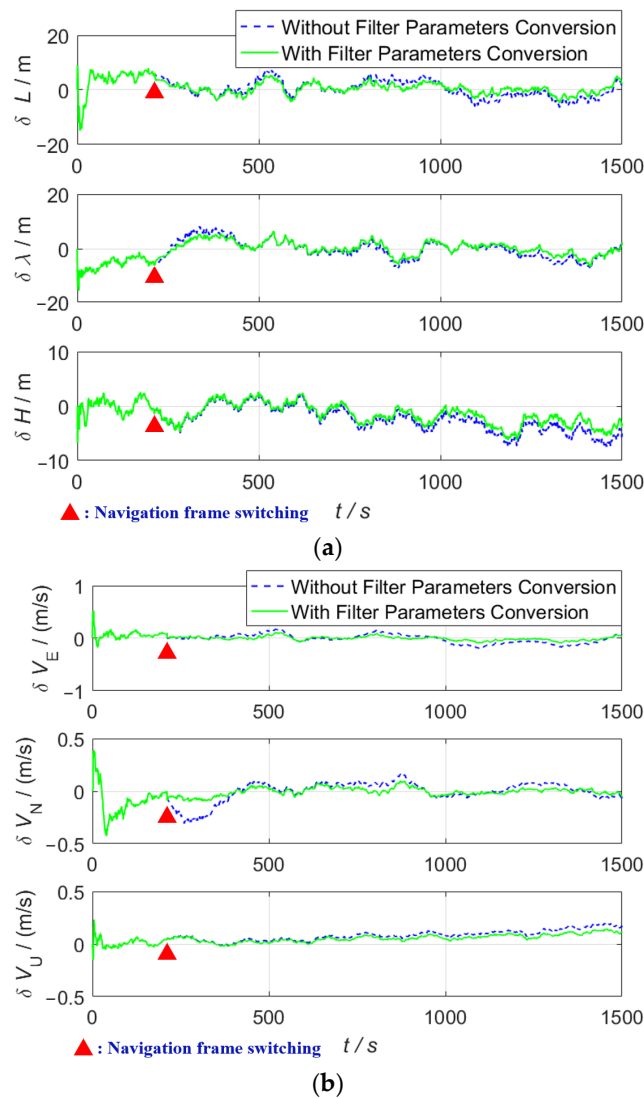


Figure 4. Cont.

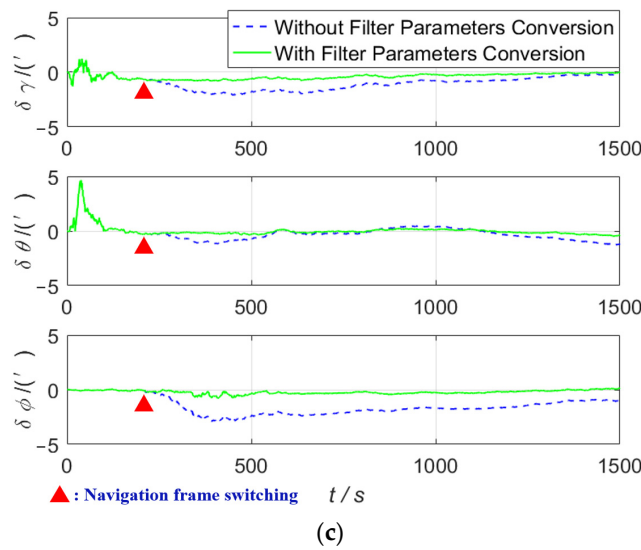


Figure 4. Error curves of the two methods: (a) position error curves; (b) velocity error curves; and (c) attitude error curves.

It can be seen from Figure 4 that the errors of multi-information fusion autonomous navigation without filter parameter conversion oscillate when entering the polar regions. In the attitude errors, the yaw error without the filter parameter conversion was the largest, and the oscillation amplitude reached up to 3'. Due to the low observability of the yaw during a uniform flight, the change in filter structure was prone to oscillation. The oscillation amplitude of the velocity error was 0.3 m/s. The oscillations in the velocity error and position error were smaller than that of the attitude error and could converge quickly. That is because the multi-information fusion autonomous navigation filter took the velocity provided by SRS and the position provided by CNS as the measurements. Therefore, the velocity and position could be corrected directly. During the conversion of the navigation coordinate frame, the errors of the multi-information fusion autonomous navigation method with the filter parameter conversion were lower, and there were no significant oscillations.

The RMSEs (root-mean-square errors) of the SINS/SRS/CNS multi-information fusion autonomous navigation with and without filter parameter conversion are shown in Figure 5.

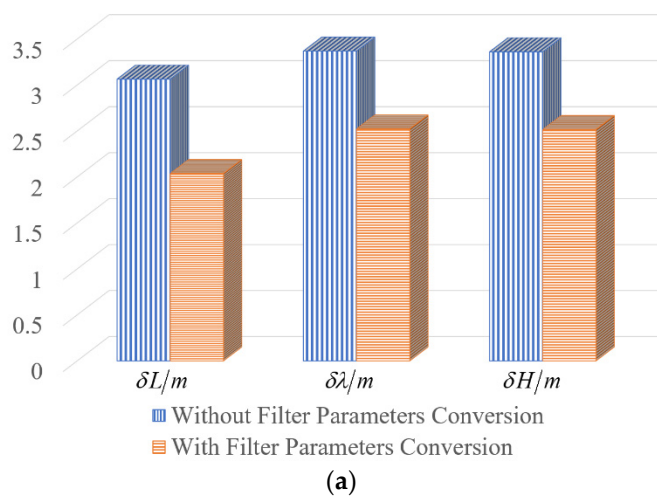


Figure 5. Cont.

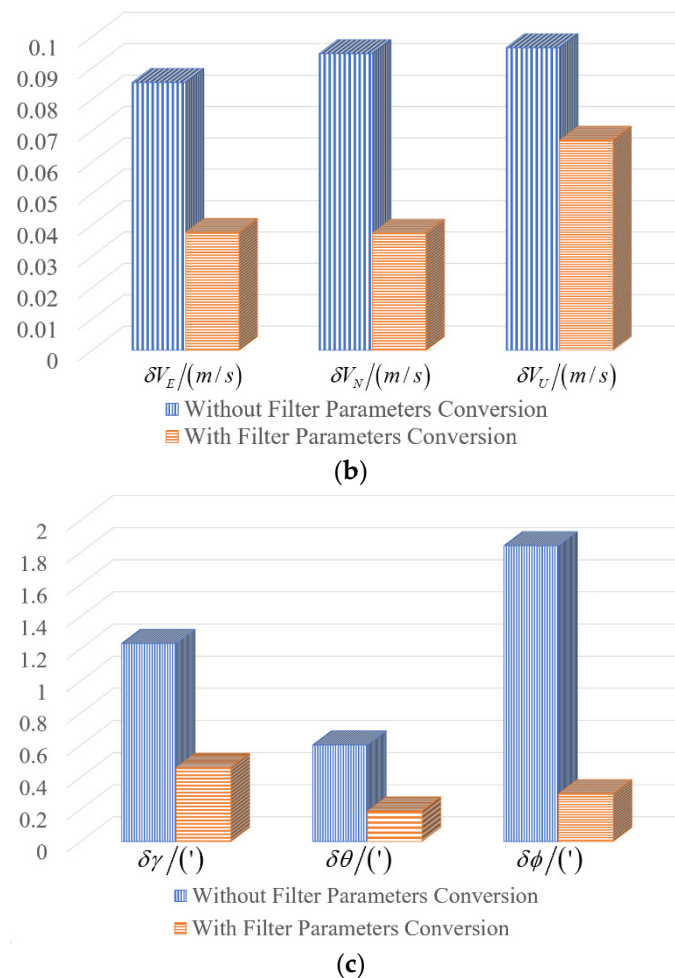


Figure 5. The RMSEs of multi-information fusion autonomous navigation: (a) the RMSEs of the position; (b) the RMSEs of the velocity; and (c) the RMSEs of the attitude.

Based on the results demonstrated in Figures 4 and 5, the navigation performance of the multi-information fusion autonomous navigation method with filter parameter conversion was better than that without filter parameter conversion. It could realize smooth switching between different coordinate frames and improve the navigation accuracy.

5.2. Experiment and Analysis

In view of the restriction of experimental conditions, actual high-altitude and long-endurance flight experiments cannot be conducted in our research center. Considering that RTK (real-time kinematics) can provide high-accuracy velocity and position, the following experimental scheme was designed. The high-accuracy velocity and position offered by RTK were taken as the true values of the SRS velocity, CNS position, and BA altitude. The CNS position error, BA altitude error, and SRS velocity error simulated in Section 5.1 could be superimposed on the true values to obtain the experimental data. On this basis, a SINS/RTK integrated navigation vehicle experiment in a natural system was conducted to verify the parameter conversion method proposed in Section 4. The experimental vehicle is shown in Figure 6.



Figure 6. The experimental vehicle.

The parameters of the vehicle experiment are listed in Table 2.

Table 2. The parameters of the vehicle experiment.

Parameters	Value
Gyro constant bias (deg/h)	0.015
Accelerometer constant bias (ug)	85
Gyro angular random walk (deg/sqrt(h))	0.0007
Accelerometer velocity random walk (ug/sqrt(Hz))	10
Horizontal positioning error (m)	20
Altitude error (m)	10
Velocity error (m/s)	0.5

The experiment trajectory is demonstrated by the red line in Figure 7. The approximate location was east longitude 118.790° and north latitude 31.939° . The navigation coordinate frame was the g frame in the beginning, and it switched to the G frame after 300 s. The transpolar navigation was imitated by coordinate system switching.

Figure 8 indicates that the filter parameter conversion method proposed in this article can achieve smooth switching between different coordinate systems without oscillation.



Figure 7. The experimental trajectory.

Figure 8 illustrates the positions generated by the different methods.

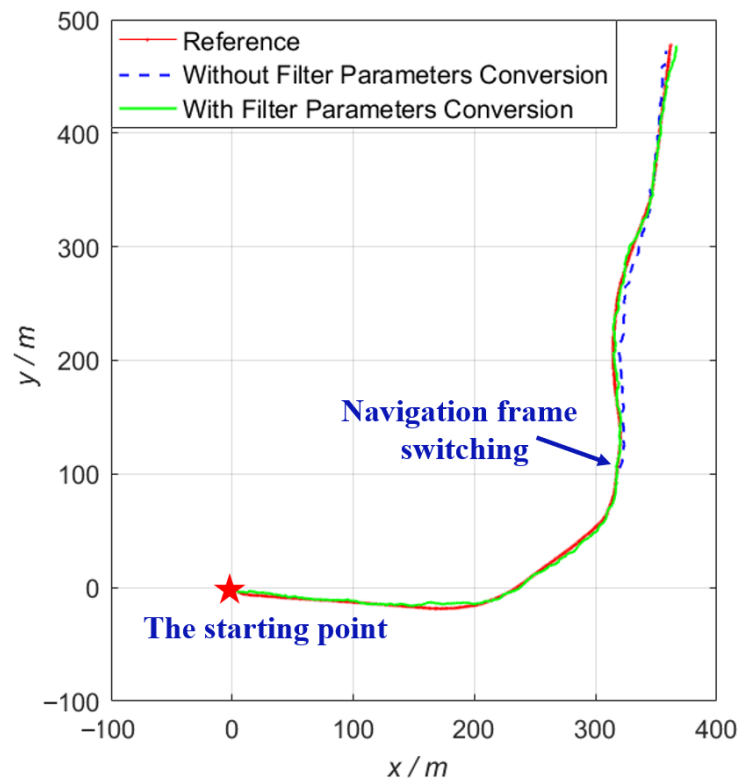


Figure 8. The positions of the two methods with and without filter parameter conversion.

The horizontal position RMSEs of these two methods are shown in Figure 9.

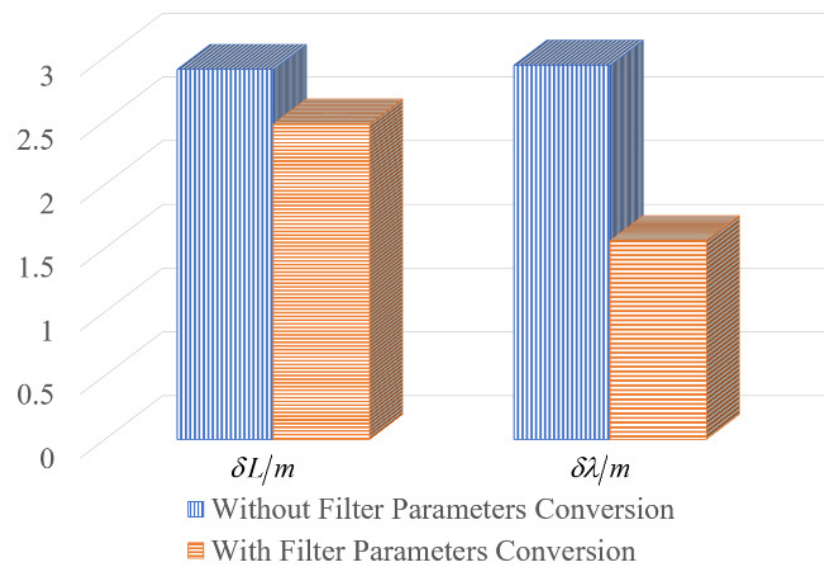


Figure 9. The horizontal position RMSEs of multi-information fusion autonomous navigation.

Figure 9 also shows that the proposed multi-information fusion autonomous navigation method with filter parameter conversion can effectively reduce the navigation errors caused by coordinate frame switching. Compared with the method without filter parameter conversion, the horizontal position accuracy of the proposed method was enhanced by about 29%.

6. Conclusions

To improve the continuity and smoothness of high-altitude and long-endurance UAV transpolar flight and to optimize autonomous navigation performance, a SINS/SRS/CNS multi-information fusion global autonomous navigation method was proposed. The system equations in the middle–low latitudes and high latitudes were established. The navigation and filter parameter conversion relationships between different coordinate frames were derived. The simulation and experiment verified that the SINS/SRS/CNS multi-information fusion global autonomous navigation method with parameter conversion can effectively improve the accuracy and smoothness and realize non-oscillation switching in transpolar navigation. In the vehicle experiment, the proposed algorithm improved the horizontal position accuracy by more than 29% compared with the multi-information fusion global autonomous navigation method without filter parameter conversion.

Author Contributions: Conceptualization, B.Z. and Q.Z.; methodology, B.Z.; software, B.Z.; validation, B.Z., Q.Z. and C.G.; formal analysis, X.Z. and W.Q.; investigation, C.G. and X.Z.; resources, J.L.; data curation, C.G. and W.Q.; writing—original draft preparation, B.Z.; writing—review and editing, Q.Z.; visualization, B.Z.; supervision, Q.Z.; project administration, J.L.; funding acquisition, J.L. All authors have read and agreed to the published version of the manuscript.

Funding: This research was funded by the National Natural Science Foundation of China (grants 61533008 and 61603181), the Postgraduate Research & Practice Innovation Program of Jiangsu Province (No. KYCX18_0268), the Qing Lan Project of the Jiangsu Higher Education Institutions (No. 2022), and the Natural Science Foundation of the Jiangsu Higher Education Institutions of China (No. 19KJD590001).

Institutional Review Board Statement: Not applicable.

Informed Consent Statement: Not applicable.

Data Availability Statement: Not applicable.

Acknowledgments: The authors would like to thank all the editors and anonymous reviewers for their helpful comments and valuable remarks.

Conflicts of Interest: The authors declare no conflict of interest.

References

1. Sheridan, I. Drones and Global Navigation Satellite Systems: Current Evidence from Polar Scientists. *R. Soc. Open Sci.* **2020**, *7*, 191494. [[CrossRef](#)]
2. Huang, L.; Xu, X.; Ge, H.R. Single-Axis Rotation Modulation Transverse SINS Based on Virtual Sphere Model in Polar Region. *IEEE Sens. J.* **2022**, *22*, 13442–13450. [[CrossRef](#)]
3. Zhao, W.Y.; Zhang, G.T.; Liu, W. Working Performance Analysis on Polar Navigation of Semi-analytical Inertial Navigation System. In Proceedings of the 2021 IEEE Conference on Telecommunications, Optics and Computer Science (TOCS), Shenyang, China, 10–11 December 2021.
4. Zhao, B.; Zeng, Q.H.; Liu, J.Y. A New Polar Alignment Algorithm Based on the Huber Estimation Filter with the Aid of BeiDou Navigation Satellite System. *Int. J. Distrib. Sens. Netw.* **2021**, *17*, 15501477211004115. [[CrossRef](#)]
5. Zhao, W.Y.; Zhang, G.T.; Liu, W. Research on High-latitude Transfer Alignment Technology. In Proceedings of the 2021 International Conference on Intelligent Computing, Automation and Systems (ICICAS), Chongqing, China, 29–31 December 2021.
6. Zhang, F.B.; Gao, X.H.; Song, W.B. A Vision Aided Initial Alignment Method of Strapdown Inertial Navigation Systems in Polar Regions. *Sensors* **2022**, *22*, 4691. [[CrossRef](#)] [[PubMed](#)]
7. Cui, W.T.; Ben, Y.Y.; Zhang, H.X. A Review of Polar Marine Navigation Schemes. In Proceedings of the 2020 IEEE/ION Position, Location and Navigation Symposium (PLANS), Portland, OR, USA, 20–23 April 2020.
8. Song, L.J.; Zhao, W.L.; Cheng, Y.X. Based on Grid Reference Frame for SINS/CNS Integrated Navigation System in the Polar Regions. *Complexity* **2019**, *2019*, 2164053.
9. Zhao, L.; Kang, Y.Y.; Cheng, J.H. A Fault-Tolerant Polar Grid SINS/DVL/USBL Integrated Navigation Algorithm Based on the Centralized Filter and Relative Position Measurement. *Sensors* **2019**, *19*, 3899. [[CrossRef](#)] [[PubMed](#)]
10. Huang, L.; Xu, X.; Zhao, H.M. Transverse SINS/DVL Integrated Polar Navigation Algorithm Based on Virtual Sphere Model. *Math. Probl. Eng.* **2020**, *2020*, 8892750. [[CrossRef](#)]
11. Zhao, C.L.; Wu, W.Q.; Lian, J.X. Research on Rotating Modulation Inertial Navigation System Error Characteristics Simulation Method in Polar Area. In Proceedings of the Guidance, Navigation & Control Conference (CGNCC), Yantai, China, 8–10 August 2014.
12. Sun, J.L.; Wu, Z.L.; Yin, Z.D. Adaptive Filtering and Temporal Alignment Based Fusion Algorithm for Navigation Systems in the Arctic Region. *IEEE Syst. J.* **2018**, *13*, 2022–2033. [[CrossRef](#)]
13. Song, L.J.; Yang, G.Q.; Zhao, W.L. The Inertial Integrated Navigation Algorithms in the Polar Region. *Math. Probl. Eng.* **2020**, *2020*, 5895847. [[CrossRef](#)]
14. Yang, S.J.; Feng, W.W.; Wang, S. A SINS/CNS Integrated Navigation Scheme with Improved mathematical horizon reference. *Measurement* **2022**, *195*, 111028. [[CrossRef](#)]
15. Tian, M. Review of Polar Integrated Navigation Algorithm. *J. Phys. Conf. Ser.* **2019**, *1213*, 032017.
16. Wei, W.H.; Gao, Z.H.; Gao, S.S. A SINS/SRS/GNS Autonomous Integrated Navigation System Based on Spectral Redshift Velocity Measurements. *Sensors* **2018**, *18*, 1145. [[CrossRef](#)]
17. Collins, J.; Conger, R. MANS-Autonomous Navigation and Orbit Control for Communications Satellites. In Proceedings of the 15th International Communications Satellite Systems Conference and Exhibit, San Diego, CA, USA, 28 February–3 March 1994.
18. Tai, F.; Noerdlinger, P.D. A Low Cost Autonomous Navigation System. In Proceedings of the Guidance and Control Conference, Keystone, CO, USA, 4–8 February 1989.
19. Gao, G.L.; Gao, S.S.; Hong, G.Y. A Robust INS/SRS/CNS Integrated Navigation System with the Chi-Square Test-Based Robust Kalman Filter. *Sensors* **2020**, *20*, 5909. [[CrossRef](#)]
20. Gao, G.L.; Gao, S.S.; Hu, G.L. Spectral Redshift Observation-based SINS/SRS/CNS Integration with an Adaptive Fault-tolerant Cubature Kalman Filter. *Meas. Sci. Technol.* **2021**, *32*, 095103. [[CrossRef](#)]
21. Chen, W.N.; Zeng, Q.H.; Liu, J.Y. Seamless Autonomous Navigation Based on the Motion Constraint of the Mobile Robot. *Ind. Robot.* **2017**, *44*, 178–188. [[CrossRef](#)]